PCCP

RSC Publishing

PERSPECTIVE

View Article Online
View Journal | View Issue

Cite this: *Phys. Chem. Chem. Phys.*, 2013, **15**, 5345

Super-resolution imaging of interactions between molecules and plasmonic nanostructures

Katherine A. Willets*

Received 1st November 2012,
Accepted 7th January 2013

DOI: 10.1039/c3cp43882a

www.rsc.org/pccp

Super-resolution far-field imaging has recently emerged as a novel strategy for imaging interactions between plasmonic nanostructures and single molecules with spatial resolution <5 nm. In these experiments, the emission centroid of a diffraction-limited spot is modeled as a two-dimensional Gaussian, allowing the position of an emitter to be determined with nanoscale precision. In this perspective, we describe the principles of super-resolution far-field imaging and then highlight its application to several different problems in plasmonics, including surface-enhanced fluorescence of ligands bound to nanoparticle surfaces, nanoparticle-mediated catalysis, and mapping electromagnetic hot spots. In all cases, the complex coupling between molecular emission and plasmon modes of the underlying nanostructure must be considered. While this complicates the interpretation of super-resolution images of plasmonic systems, the coupling also opens new doors for understanding the fundamental interactions between molecules and plasmonic nanostructures.

Introduction

The development of plasmonic materials has revolutionized fields as diverse as nanomedicine,[1,2] biosensing,[3–5] catalysis,[6,7] photothermal therapy,[8] homeland security[9] and art restoration.[10] In many of these applications, the interaction between a noble metal nanostructure and a nearby analyte molecule drives the measured signal response. For example, surface-enhanced Raman scattering, or SERS, occurs when a molecule is located in the region of sizable electromagnetic field enhancement on the nanoparticle surface; the locally enhanced electromagnetic fields lead to dramatic increases in both the excitation and Raman scattering intensity from the molecule.[11] Surface-enhanced fluorescence, or SEF, benefits from similar signal enhancements, although the molecule must be positioned further from the nanoparticle surface, in order to prevent fluorescence quenching.[12] In both cases, the location of the molecule relative to the plasmonic nanostructure will dictate the magnitude of the measured signal response.

Researchers have long accepted the model of electromagnetic "hot spots," which correspond to the regions on the nanoparticle surface where the electromagnetic fields are most strongly enhanced.[13–15] Electromagnetic field enhancements occur when surface plasmons are excited in materials with both a negative real and small positive imaginary dielectric constant.[16] Plasmons are light-driven collective oscillations of the surface conduction electrons in these materials and can either be localized or propagating in nature. Materials that support localized surface plasmons are smaller than the wavelength of the excitation light, *e.g.* nanoparticles, and the oscillating electron density wave is effectively confined near the nanoparticle surface. On the other hand, propagating plasmons occur in either thin metal films or structures with at least one dimension that is longer than the wavelength of the exciting light, such as nanowires. In propagating plasmons, the oscillating electron density wave can travel many microns from the excitation site. In both localized and propagating surface plasmons, local electromagnetic field enhancements are induced, which have critical implications for surface-enhanced spectroscopies, such as SERS and SEF.

When molecules are positioned in regions of electromagnetic enhancement on or near a plasmonic nanostructure, the measured signal can be enhanced by many orders of magnitude relative to the non-enhanced counterpart.[11,12] This is due, in part, to the excitation of the molecule by the plasmonically-enhanced electromagnetic field, but is also due to coupling between the emission from the molecule and the plasmon modes of the underlying nanostructure. While the concept of plasmon-enhanced emission is well-known—for example, SERS is typically referred to as an E^4 enhancement mechanism, given that both the excitation intensities and emission intensities are enhanced—understanding this process at the nanoscale level is especially challenging.[17] Given the small size of the coupled

Department of Chemistry and Biochemistry, The University of Texas at Austin, Welch Hall 2.204, 105 E. 24th St. STOP A5300, Austin, Texas 78712-1224, USA. E-mail: kwillets@cm.utexas.edu; Fax: +1 512 471 0985; Tel: +1 512 471 6488

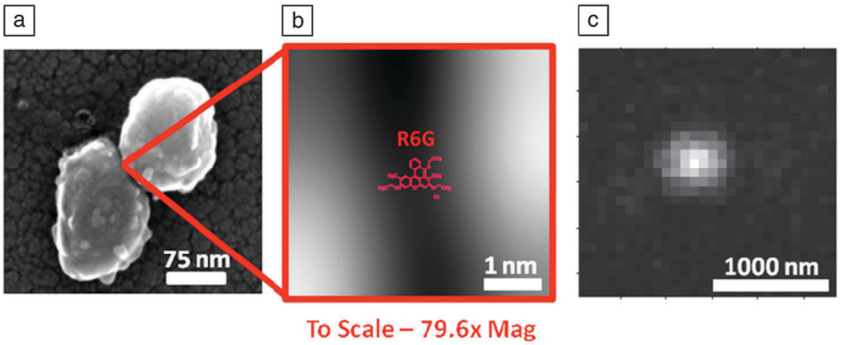

Fig. 1 (A) SEM image of a SERS-active nanoparticle dimer. (B) Zoomed-in image of (A) showing the relative size of an R6G molecule compared to the gap between the adjacent nanoparticles. (C) Example of a diffraction-limited spot. Reproduced with permission from ref. 28. Copyright (2012) Materials Research Society.

nanoparticle–molecule system, in which both components are much smaller than the wavelength of light, features of both the nanostructure and the molecule cannot be resolved in a far-field optical microscope (Fig. 1). As a result, it is impossible to resolve the location of the molecule and determine how its position on the nanoparticle surface influences its coupling to the underlying plasmonic substrate.

Recently, super-resolution far-field imaging has been applied to problems in plasmonics—specifically, the interaction between molecules and plasmonically-enhanced electromagnetic fields.[7,18–28] Super-resolution far-field imaging was developed by the fluorescence community as a way to overcome the optical diffraction limit; while far-field optical microscopy produces images with resolution of ~200–400 nm, super-resolution techniques overcome this fundamental resolution limit and can provide <5 nm resolution.[29,30] In this perspective, we discuss the basic principles of super-resolution imaging and provide several examples of how this imaging technique yields new insight into the interaction between plasmonic nanoparticles and nearby emitting molecules. Although there are several additional examples in the literature that use super-resolution imaging to track the location of individual nanoparticles based on their Rayleigh scattering,[31,32] we focus here on studies highlighting the interaction between molecules and plasmonic nanoparticles. We also note that other approaches are available for overcoming the diffraction-limit of light, such as stimulated emission depletion (STED) and structured illumination microscopy.[33] These techniques achieve improved resolution through the use of modified illumination sources, but are still in the early phase of development for plasmonic applications, with most of the current literature focused on theoretical simulations.[34–36] As such, we will focus here on super-resolution imaging, as defined below.

Super-resolution imaging

Super-resolution far-field imaging is effectively the combination of two principles: super-localization microscopy and active control of the emissive state of a molecule.[37] In standard far-field optical microscopy, an object that is smaller than roughly half the wavelength of light will appear as a diffraction-limited spot on a detector, as shown in Fig. 1C. The actual size and shape of the diffraction-limited image is dictated by the point spread function (PSF) of the microscope, which describes how the image of the emitting species is distorted by the imaging system. The PSF can be approximated by a model function, such as a two-dimensional Gaussian, as shown in eqn (1).[38,39]

$$I(x,y) = z_0 + I_0 e^{\left[-\frac{1}{2}\left[\left(\frac{x-x_0}{s_x}\right)^2+\left(\frac{y-y_0}{s_y}\right)^2\right]\right]} \quad (1)$$

In this expression, the spatially-dependent intensity of the diffraction-limited spot ($I(x,y)$) is a function of the background signal, z_0; the peak intensity of the spot, I_0; the location of the peak intensity, x_0 and y_0; and the width of the spot in the x- and y-dimensions, s_x and s_y respectively. By fitting a PSF to eqn (1), the centroid position (x_0, y_0) can be determined. Super-localization microscopy assumes that the location of the emitting species corresponds to the calculated centroid position, which means that the position of the emitter is known with precision much better than the width of the original diffraction-limited spot.[39] Typically, the location of the emitter can be determined with (theoretical) resolution better than 5 nm in the case of plasmonically-enhanced signals, based on the number of emitted photons, the width of the fitted Gaussian (s_x and s_y in eqn (1)), the size of the pixels in the imaging CCD, and the noise of the background.[23,39]

In the case when multiple emitters are active at the same time, the PSFs of the individual emitters will be superimposed, and the calculated centroid will be a superposition of the locations of all emitting species. To overcome this and resolve the locations of individual emitters, we need the emission to modulate with time, such that only a single emitter is active, or "on," at a given time. In the fluorescence community, there are myriad strategies for controlling the "on" state of an emitter, including successive photobleaching of closely-spaced probe molecules,[40] using photoswitchable probes that change state upon interacting with light,[29,30] shelving populations of molecules in the triplet state,[41,42] or exploiting the inherent "blinking" exhibited by many emissive species.[43] As individual emitters turn on, the PSF is fit and the centroid position is determined. By repeating this process over many emission events, the position of each individual emitter in a population is determined, and an image is constructed by plotting all of the calculated centroid positions. The combination of super-localization

microscopy and modulated emission are the hallmarks of true super-resolution far-field imaging. This process has proven to be extremely powerful in biological systems, where cellular structures are labeled with multiple fluorescent dyes, each one is individually localized, and then the centroids are plotted to reconstruct the shape of the underlying cellular structure.[29,30] In plasmonic systems, the reconstructed images are less straightforward due to the coupling between each emission event and the underlying plasmon modes of the nanostructure, and will be discussed in more detail below.

Experimental considerations

The specific experimental details for the experiments described herein can be found in the original citations; however, there are several common themes. Nearly all super-resolution imaging experiments are performed in a wide field excitation geometry, in which the excitation spot is typically several microns in diameter.[44] For the experiments performed in the author's lab, the excitation is introduced *via* epi-illumination through a high numerical aperture (NA) oil immersion objective. The high NA allows for the smallest possible diffraction-limited spot, as optical resolution is limited to 0.61λ/NA, based on the Rayleigh criterion. The Raman scattered light is collected through the same objective (*e.g.* backscattering geometry), appropriately filtered to reject any Rayleigh scattered excitation light, and then passed to an imaging CCD, to produce a two-dimensional diffraction limited image, such as the example shown in Fig. 1C. The image must be projected onto the CCD at sufficient magnification such that the diffraction-limited spot extends over multiple imaging pixels to prevent over-pixilation of the image and increased uncertainty in the centroid fit.[39] In most of our work, a beamsplitter is used to send half of the emission to a spectrometer equipped with a liquid-nitrogen cooled CCD, allowing for simultaneous imaging and spectroscopy.[20–22] Having spectral information that is correlated with the measured images is especially important for SERS imaging, in which the identity of the emitting analyte can be determined by the signature vibrational modes of the species. However, care must be taken in selecting the image splitting optic, as any polarization artifacts introduced by this optic can further distort the PSF.

The final step of the experiment is fitting the measured PSF to the chosen model function. A 2-dimensional Gaussian function (eqn (1)) is the most straightforward fitting function; however, this choice of function is an imperfect model for the PSF and may introduce associated uncertainty to the localization accuracy of the fits, as is well-known in the single molecule fluorescence community.[45,46] While this is handled in the fluorescence community by modeling the PSF as a dipole emitter, the coupling between a molecule and a plasmonic nanostructure complicates the analysis. Uji-i and coworkers performed finite-difference time domain calculations showing how the angular distribution, and thus the PSF, of an emitting dipole is perturbed when placed near the surface of a plasmonic nanowire (Fig. 2).[24] Based on the position of the emitter on the nanostructure surface, the PSF can be highly distorted, and it is clear that a Gaussian is an insufficient model for fitting these data. Moreover, the plasmon-coupled emission centroid will not reflect the actual position of the molecule, given the distortion of the emission PSF induced by the nanostructure. Nonetheless, this model is still the current standard in the literature, and all of the data presented in this review use eqn (1) for super-localization fits. As super-resolution imaging gains traction in the plasmonic community, we expect new models to be developed, which will improve both the quality of the fits and the localization accuracy in super-resolution data.

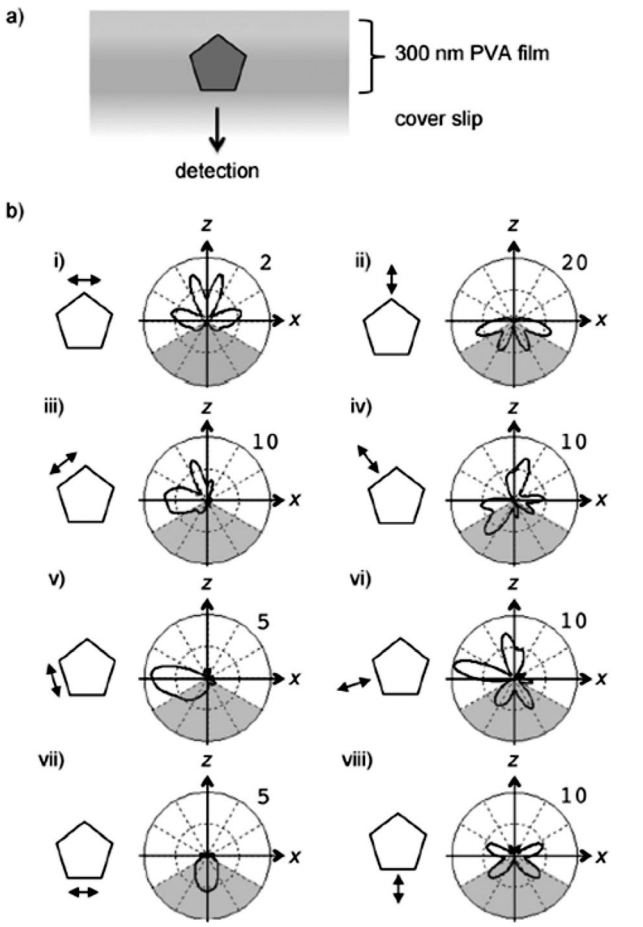

Fig. 2 Calculated far-field scattering distribution as a function of the position of an emitting dipole relative to a plasmonic nanoparticle. (A) Sample geometry used in the calculations. (B) Scattering distributions as a function of dipole position. The gray shaded region represents the collection angle of a 1.3 NA objective. Reproduced with permission from ref. 24. Copyright (2012) Wiley-VCH Verlag GmbH & Co. KGaA, Weinheim.

Super-resolution imaging of fluorescent ligands on plasmonic nanostructures

Since super-resolution imaging originated in the fluorescence community, extending these techniques to fluorescently-labeled nanostructures is a natural progression. Several recent examples in the literature have used super-resolution imaging to study

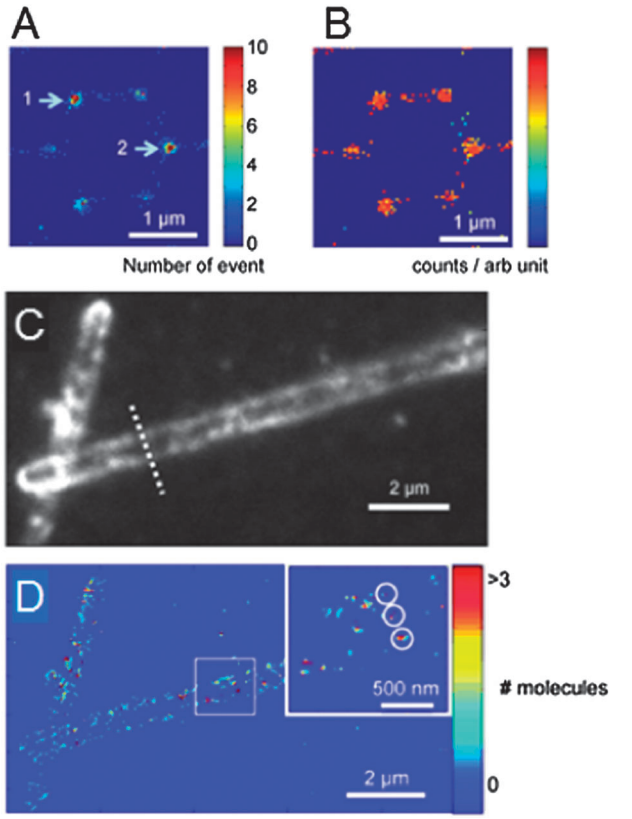

Fig. 3 Super-resolution images of Dronpa-labeled gold nanotriangles prepared by NSL. (A) Histogram showing the frequency with which the emission centroid is fit to a particular 24 × 24 nm^2 bin. (B) Histogram showing the maximum fluorescence intensity associated with each bin from (A). (C) Wide-field image of a Dronpa-labeled silver nanowire. (D) Histogram showing the frequency with which the emission centroid is fit to a particular 48 × 48 nm^2 bin for the nanowire in (C). The images are scaled to have common 2 μm scale bars. Reproduced with permission from ref. 24. Copyright (2012) Wiley-VCH Verlag GmbH & Co. KGaA, Weinheim.

fluorescently-labeled ligands bound to the surface of plasmonic nanostructures. In the first example from Lin *et al.*, a photoswitchable fluorescent protein, Dronpa, is covalently attached to the surface of various nanostructures using a biotin/avidin/biotin/antibody/Dronpa linking strategy.[24] This linking chemistry is intended to space the fluorescent protein far enough from the metal surface to suppress fluorescence quenching. Dronpa is an example of a photoswitchable probe that is activated to its "on" state *via* 405 nm light, and then probed by 488 nm excitation. By adjusting the intensity of the 405 nm activation light, the average number of molecules in the "on" state can be controlled, allowing individual fluorescent bursts to be imaged and fit to eqn (1).

Fig. 3 shows super-resolution image data from Dronpa-labeled gold nanotriangles fabricated *via* nanosphere lithography (NSL).[24] NSL produces arrays of triangles distributed in a hexagonal pattern, which typically cannot be resolved using traditional far field imaging due to the close inter-particle spacing.[47] While the spacing of the triangles in this particular array is ~1 μm, which might allow the relative positions of the triangles to be observed with standard far-field imaging, the actual size of the nanostructures would be obscured. However, by fitting the centroid position of a series of fluorescent bursts from the attached Dronpa proteins, the authors were able to determine both the size and spacing of the individual triangles in the array, which was confirmed by atomic force microscopy (AFM). In Fig. 3A, the calculated centroids were binned into a histogram that illustrates the frequency with which a fluorescent event occurred in a particular 24 × 24 nm^2 region in space. Not only does this image show how the triangles are spatially distributed with respect to one another, but it also reveals that the triangles labeled 1 and 2 showed much higher activity than the other four triangles in the unit cell. On the other hand, when the maximum fluorescence intensity associated with the data in each bin is plotted, as in Fig. 3B, the fluorescence is uniform across all six triangles; this suggests that the enhanced activity in Fig. 3A is not plasmon-mediated, but is instead due to differences in ligand binding on each individual nanostructure. The authors also noted that the fluorescence from non-specifically bound Dronpa proteins, randomly adsorbed to the glass substrate, was half as intense as the proteins bound to the metal nanostructures, indicating the presence of SEF for Dronpa bound to the gold nanotriangles.

In that same study, Dronpa-labeled silver nanowires were also imaged, albeit with dramatically different results, as shown in Fig. 3C and D.[24] Although the silver nanowires were 200 ± 50 nm in diameter, the super-resolution images (Fig. 3D) showed nanowire widths of ~550 nm, in near agreement with the raw diffraction-limited images (Fig. 3C). One possible explanation for this discrepancy is the distortion of the PSF due to the nearby nanowire, as shown in Fig. 2. If the nanowire is distorting the angular distribution of the emitted light, the localization accuracy of the fit could be compromised, introducing errors of >100 nm.[46] This loss of localization accuracy underscores one significant challenge of using super-resolution imaging with plasmonic nanostructures—that is, the inherent coupling between the emitting species and the nearby metallic structure.

For comparison, Fig. 4 shows recent work from our lab in which we generated super-resolution images of gold nanowires (69 ± 12 nm in diameter), reconstructed from fluorescently-labeled DNA covalently attached to the surface of the nanowires.[18] In this example, the DNA was labeled with carboxytetramethyl rhodamine (TAMRA), which can be efficiently shelved in a dark triplet state, with a stochastic return to the emissive state that is controlled by the excitation intensity. As with the work from

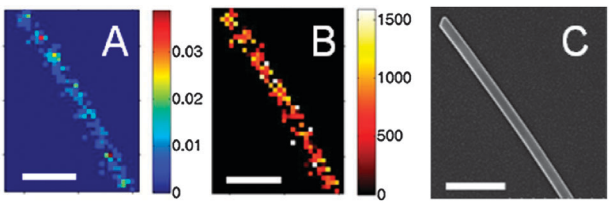

Fig. 4 Super-resolution images of TAMRA-DNA-labeled gold nanowires. (A) Histogram showing the frequency with which the emission centroid is fit to a particular 40 × 40 nm^2 bin. (B) Histogram showing the average fluorescence intensity associated with each bin from (A). (C) SEM image of the nanowire. Adapted from ref. 18. Copyright 2013 from the PCCP Owner Societies.

Lin *et al.*, individual fluorescent bursts were identified and fit to eqn (1) to generate a series of centroid values. The centroid values were binned to create a frequency histogram (Fig. 4A), and the average intensity of all points within a given bin were plotted to create an intensity histogram (Fig. 4B). In contrast to the data in Fig. 3D, the reconstructed images showed excellent agreement with the dimensions of the underlying nanowire, as shown in the accompanying scanning electron microscope (SEM) image shown in Fig. 4C.[18]

Although we found strong agreement between the size and shape of the reconstructed images and the shape of the nanowire, we also noticed that some of our frequency histograms showed increased burst activity at the nanowire ends. Our initial instinct was that we had increased fluorophore labelling at the nanowire end, much like the heterogeneous triangle labelling seen in Fig. 3A. However, we also found several examples in which the emission centroids were strongly localized, with emission only appearing at specific locations along the length of the nanowire. Correlated structure studies revealed that the site-specific emission was associated with small nanoparticles attached to the sidewalls of the nanowire. This observation led us to speculate that much of the fluorescence emission in our studies was coupling into propagating surface plasmon modes in the nanowire.[48,49] In the case when nanoparticle defects were present, the plasmon-coupled emission light was scattered preferentially at those defect sites, while in other cases, the plasmon-coupled emission was scattered preferentially at the nanowire ends. This coupling between fluorescence emission and propagating plasmons suggests that the calculated centroids are not associated with the actual location of the excited TAMRA dye—instead, the TAMRA and the observed emission could be many nanometres or even microns apart.

Our results, in conjunction with the data from Lin *et al.*, highlight the complexity of the interactions between single molecules and plasmonic nanostructures. Unlike super-resolution imaging studies in biological systems, where the localized centroid position of the emission most likely correlates in a one-to-one fashion with the actual position of the emitter, the presence of plasmonic nanostructures can perturb the emission centroid in diverse and challenging ways. Regardless of whether the PSF is distorted by the presence of the metal or is emitted elsewhere due to emission coupling into the plasmon modes of the nanostructure (or even a combination of the two), we cannot ignore the importance of the plasmon modes when interpreting super-resolution imaging data on plasmonic nanostructures.

Super-resolution imaging of catalytic activity

Super-resolution fluorescence imaging has also proven a useful tool for studying catalytic activity on the surface of plasmonic nanoparticles.[7,26,27] In these studies, a non-fluorescent species reacts at the nanoparticle surface to produce a fluorescent product—specific examples include the reduction of resazurin to resorufin[27] or the oxidative deacetylation of Amplex Red to resorufin.[7] Each product resorufin molecule produces a strong burst of fluorescence at the nanoparticle surface, which can be localized by fitting its PSF to eqn (1) above. Because each product molecule is generated stochastically at the nanoparticle surface, the frequency of product turnover can be controlled through the concentration of available substrate molecules; this introduces the "active control" of emission element that is critical for super-resolution studies.

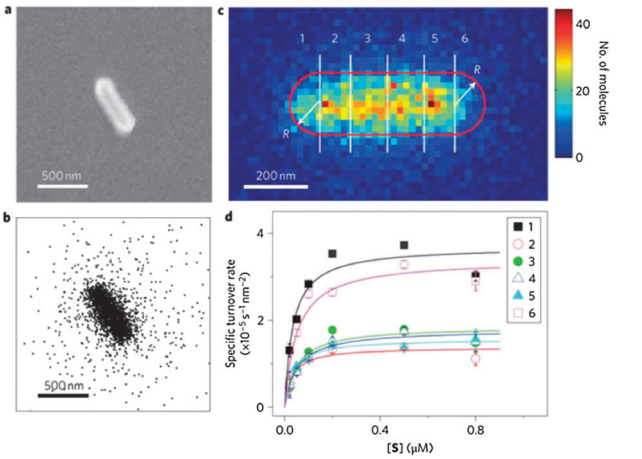

Fig. 5 (A) SEM image of a catalytically-active gold nanorod. (B) Super-resolution image showing the centroid position of individual catalytic turnover events at the nanorod surface. (C) Histogram showing the frequency with which the emission centroid is fit to a particular 20 × 20 nm^2 bin. The nanorod is broken into 6 regions. (D) Specific turnover rate for each region (1–6) of the nanorod as a function of substrate concentration. Reprinted by permission from Macmillan Publishers Ltd: Nature Nanotechnology (ref. 7), copyright (2012).

Fig. 5 shows an example of the oxidative deacetylation of Amplex Red to resorufin at the surface of a porous silica-coated gold nanorod.[7] Using super-resolution imaging, the shape of the nanorod (Fig. 5A) can be reconstructed by mapping the centroid positions of each fluorescent burst from resorufin (Fig. 5B). The centroids are then binned into 20 nm × 20 nm bins (Fig. 5C) to study the specific turnover rate—that is, the frequency of the product bursts per unit time per catalyst surface area—at different sites along the nanorod surface. The nanorod is further divided into six individual segments in order to probe the catalytic activity as a function of nanoparticle shape. In Fig. 5D, the specific turnover rate is plotted for all six segments as a function of the Amplex Red concentration. This figure shows that there is a clear difference between the turnover rate at the end of the nanorod *versus* the middle. Using the specific turnover rate and the concentration of Amplex Red, a catalytic rate constant is calculated and shows that different rods have distinct reactivity patterns, with the majority showing enhanced catalytic activity at the nanorod ends, but a small population showing suppressed catalytic activity at the ends relative to the center. The authors noted that the catalytic rate constant was not only (on average) higher at the nanorod ends, but was also higher for shorter nanorods than longer nanorods.

The shape-dependent catalytic activity decided above would be completely lost in a ensemble-averaged experiment, in which each turnover event would appear as a single diffraction-limited spot. The super-resolution analysis enables individual turnover

events to be spatially localized, and allows reaction kinetics to be analyzed in a site-specific manner with respect to the nanorod shape and size. The enhanced activity at the end of the nanorods, as shown by this experiment, is consistent with the mechanism that nanorod ends are associated with low-coordination metal sites, and act as defect sites that promote catalytic activity. One interesting element of these experiments is the issue of the excited plasmon: 532 nm light is used to probe the fluorescence of the resorufin, but it is also resonant with the transverse plasmon mode of the gold nanorods.[50] Recent reports have shown that transverse plasmons can be transformed into longitudinal plasmons *via* hot electrons, which would result in locally enhanced electromagnetic fields at the nanorod surface.[51] Moreover, hot electrons have been implicated in photochemical reactions on nanoparticle surface for a number of years.[52] While the shape-dependent catalytic activity presented here is consistent with structure-based defects, it is intriguing to consider the possibility that plasmon excitation might also contribute to enhanced catalytic activity on nanostructure surfaces.[53] Super-resolution imaging offers a unique strategy for probing these issues in order to better understand how molecules interact with these catalytic plasmonic nanostructures with nanoscale resolution.

Super-resolution imaging of plasmonic "hot spots"

Perhaps one of the most powerful applications of super-resolution imaging of plasmonic nanostructures is the ability to map out the local electromagnetic field enhancements associated with "hot spots."[19–23,25] While near-field scanning optical microscopy (NSOM) approaches have verified the existence of regions of enhanced electromagnetic fields, the scanning probe offers limited spatial resolution ($\sim$15 nm) and is potentially perturbative to the plasmon modes of the nanostructure under study.[54–56] On the other hand, super-resolution imaging uses a molecular analyte as a probe, allowing us to study how single dipoles interact with plasmon modes of nanostructures, while providing $<$5 nm spatial resolution.

To date, two different approaches have been used to map out plasmonic hot spots in nanostructures.[19,25] The first approach is based upon single molecule SERS (SM-SERS).[19,21,22] SM-SERS is characterized by inherent intensity fluctuations, providing the signal modulation requirement for super-resolution imaging.[57–59] By tagging randomly-aggregated colloidal silver nanoparticles with a single Rhodamine 6G (R6G) molecule, our group was able to track how both the spatial origin and intensity of the SM-SERS signal from the R6G changed over time.[19,21] At the same time, we also isolated the spatial origin of a weak luminescence signal from the silver nanoparticle aggregate by exploiting the intensity fluctuations of the SM-SERS signal.

Fig. 6, A and B, shows two examples of SM-SERS spatial intensity maps, in which we bin the centroid values into 4.6 nm $\times$ 4.6 nm bins and then plot the average SERS intensity for all points within each bin.[19] We arbitrarily set the average position of the

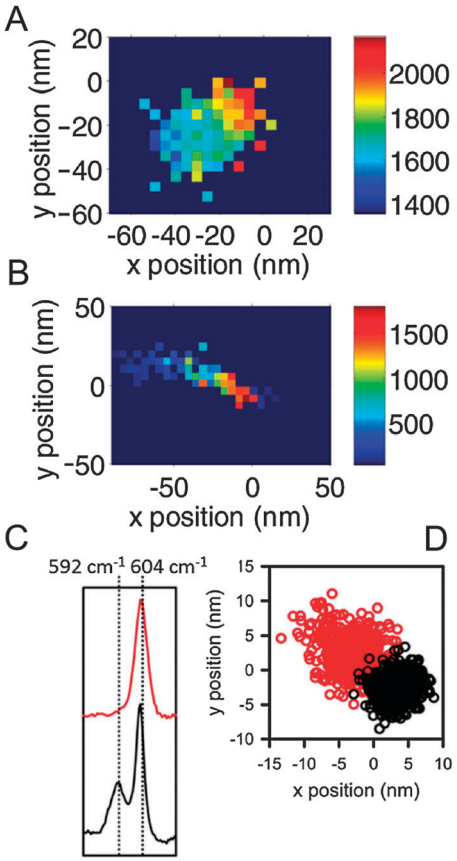

Fig. 6 (A and B) Hot spot maps showing how the average SM-SERS intensity from a SERS-active nanoparticle is spatially distributed. Bin size is 4.6 $\times$ 4.6 nm^2. (C) Spectra from an isotope-edited study showing that initially both R6G and R6G-d4 are emitting (black), followed by loss of R6G-d4 emission (red). (D) Calculated SERS centroids associated with the data from (C). The centroid shifts 8 nm from the time when both R6G and R6G-d4 are emitting (black) to the time when only the R6G is emitting (red). Adapted with permission from ref. 19 and 20. Copyright (2010 and 2012) American Chemical Society.

silver luminescence centroid at (0,0) in these images. These images show that the strongest SERS is observed when the SERS centroid is located near the luminescence centroid, and that the SERS intensity decreases in a directional, gradient fashion as the centroid moves away from that "hottest" spot. This decrease in SERS intensity is consistent with our expectations of how electromagnetic field enhancements decay away from junctions between adjacent nanoparticles, with the strongest enhancement predicted directly in the junction and a decreasing enhancement further from the junction.[60,61] The size of both hot spots also extend well above our theoretical resolution of 2–5 nm, indicating that the hot spot is not the size of a single molecule, but rather extends over tens of nanometers. These spatial intensity maps suggest that a mobile molecule is mapping out the local electromagnetic field enhancement and reporting its location through a shift in the SERS centroid and a corresponding change in SERS intensity.

One challenge with this model is proving that it is indeed the changing position of the molecule that generates the shift in the SERS centroid. Because the SERS emission is coupled

into and re-radiated by the plasmon modes of the underlying nanostructure, one would expect the excited plasmon mode to dictate the position of the emission centroid, rather than the molecule. In this case, we hypothesized that the position of the molecule must affect how the SERS couples into different plasmon modes of the nanostructure, which leads to small but measurable shifts in the plasmon-radiated emission. This hypothesis was supported by theoretical calculations from Ausman and Schatz that showed that the changing position of a nearby emitting dipole changes the near-field emission pattern of a radiating plasmonic structure.[62]

To test whether the position of the molecule is, in fact, capable of shifting the measured centroid, we performed studies in which we increased the average number of analytes on the nanoparticle aggregate surface from ~1 to ~3–5.[20] We also used a mixture of R6G and a deuterated analog (R6G-d4), in order to spectroscopically distinguish the two emitters.[59] Fig. 6C shows an example in which SERS was initially observed from both the R6G and the R6G-d4, as evidenced by the presence of a spectral peak at 604 cm^{-1} (R6G) and 592 cm^{-1} (R6G-d4). The associated SERS centroid positions are shown as the black data in Fig. 6D. After ~45 seconds, the emission from the R6G-d4 turned off, as shown in the red spectrum in Fig. 6C. At the same time, the corresponding SERS centroid showed a ~8 nm shift in its position (red data, Fig. 6D). If the plasmon modes of the nanoparticle were exclusively dictating the centroid, then we would not expect the centroid to shift as the R6G-d4 become non-emissive; however, given the change in the centroid when the molecule turns off, we can conclude that the position of the molecule does, indeed, influence the measured SERS centroid. However, we emphasize that the SERS centroid does not represent the absolute position of the molecule on the nanoparticle surface. Instead it represents how the plasmon modes of the nanoparticle re-radiate the Raman scattering from a nearby dipole.

A second strategy for mapping plasmonic hot spots is based on SEF.[25] In work from Cang *et al.*, plasmonic substrates are incubated in a dilute solution of fluorescent dye (Chromeo 642). When the dye diffuses into the hot spot, a burst of fluorescence is observed on the CCD camera. The PSF of each fluorescent burst is fit to eqn (1) to extract the emission centroid. As with the SERS data, a plot is constructed relating the intensity of the fluorescence to the spatial origin of the signal; two examples are shown in Fig. 7. In Fig. 7A, the hot spot is associated with a thin aluminum film, while in Fig. 7B, the hot spot is associated with a randomly aggregated silver nanoparticle cluster. Despite the different substrates, both hot spots show a region of strong intensity (the ''hottest'' spot), accompanied by a gradient decay in intensity as the centroid position moves away from that spot. Moreover, the sizes of the hot spots extend over tens of nanometers, as with the SERS hot spot maps above.

Both sets of data challenge the notion that a single molecule must be sitting directly in a junction between adjacent nanoparticles to be detected. Given the extended size of the hot spots mapped out in both the SERS and the SEF studies,

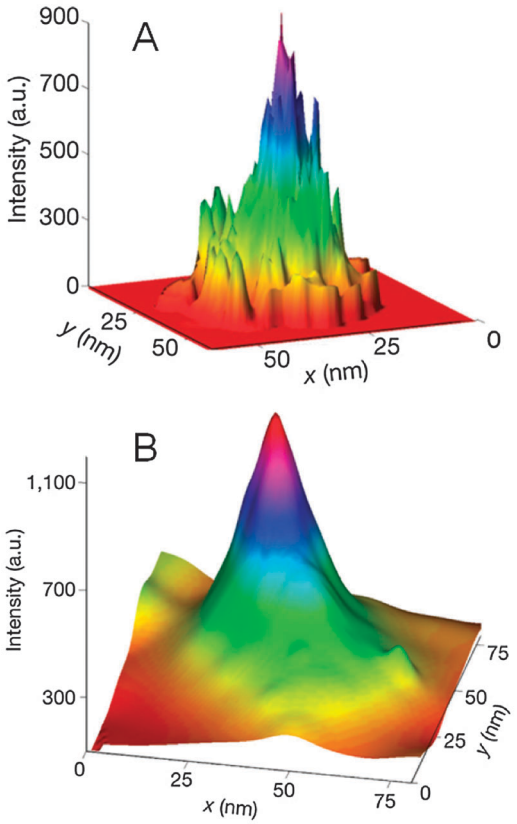

Fig. 7 Hot spot maps showing how the SEF intensity is spatially distributed from an (A) aluminum thin film and (B) silver nanoparticle aggregate. Adapted by permission from Macmillan Publishers Ltd: Nature Nanotechnology (ref. 25), copyright (2012).

super-resolution imaging reveals that surface-enhanced emission can extend tens of nanometers from the region of highest electromagnetic enhancement. The shapes of the hot spot maps are consistent with theoretical models, which show that electromagnetic field enhancement on nanoparticle surface is highly dependent on nanoparticle structure, with the strongest enhancements occurring in junctions between adjacent nanoparticles.

To determine whether the shape of the measured hot spot maps agree with the nanostructure of the underlying substrates, we turn next to correlated optical and structural studies.[21,22] For this work, our lab used alphanumerically patterned grids on indium tin oxide-coated coverglass to perform both optical and scanning electron microscopy (SEM). Fig. 8 shows an example of correlated SM-SERS super-resolution imaging data along with the nanoparticle structure.[22] In Fig. 8A, a spatial intensity map is calculated from the measured SERS centroids and the corresponding SERS intensity from a SM-SERS-active nanostructure; as before, we observe a region of highest SERS intensity, accompanied by a gradient and directional decay in the SERS signal away from the high intensity edge. The SEM image shown in Fig. 8B reveals that the nanoparticle is a trimer, with two potential SERS-active junctions. However, if we compare the spatial intensity map to the structure of the nanoparticle aggregate, we note that the alignment of the high intensity edge in the

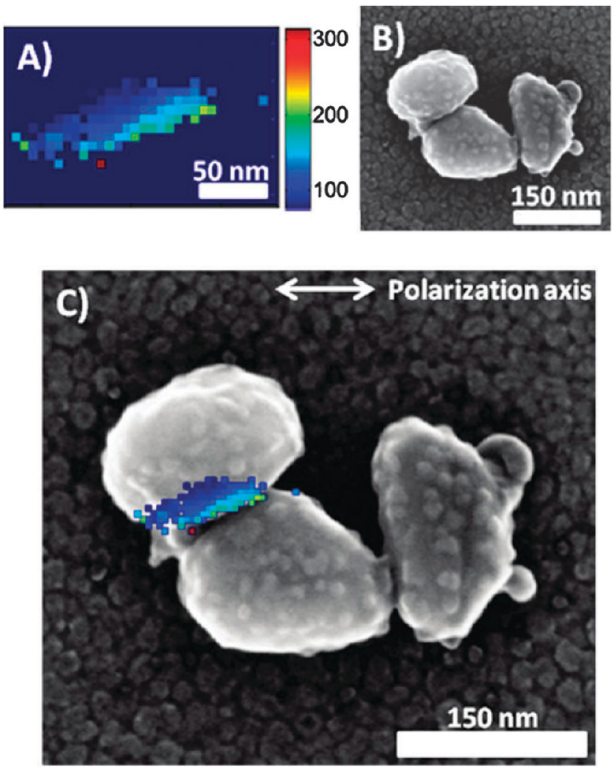

Fig. 8 (A) SM-SERS hot spot map and (B) correlated SEM image of the SERS-active nanoparticle trimer. (C) Qualitative overlay of the hot spot map from (A) on the SEM image from (B). Adapted with permission from ref. 22. Copyright (2011) American Chemical Society.

spatial intensity map is in near perfect agreement with the alignment of the junction region between the leftmost nanoparticles. To demonstrate this, we overlay the spatial intensity map on the leftmost junction in Fig. 8C. Not only does the size and shape of the spatial intensity map agree with the size and shape of the nanoparticle junction, but the intensity gradient agrees with our expectations from theory. As expected, the highest SERS occurs closest to the nanoparticle junction, and the intensity decays as the molecule explores regions further from the junction. Again, we emphasize the location of the centroid does not reflect the absolute position of the molecule, but rather how the SERS emission is coupled into the plasmon modes of the nanoparticle substrate. Nonetheless, the remarkable agreement between the spatial intensity map and the nanoparticle structure indicates that the mobile molecule does appear to be mapping out the hot spot. Later work in which we used the discrete dipole approximation to calculate the centroid location based upon local electric field enhancements verified our hot spot assignments.[21]

These studies show that super-resolution imaging is uniquely capable of probing electromagnetic hot spots with <5 nm resolution, using both SERS and SEF. As before, the challenge remains in the interpretation, given the convolution between the exact location of the emitting molecule and the coupling of the emission into the plasmon modes of the nanostructure. Despite this challenge, super-resolution imaging shows excellent agreement with local electromagnetic field enhancements measured by scanning probe techniques, showing that this approach is highly complementary to existing imaging approaches.

Conclusions and future directions

Having demonstrated that super-resolution imaging is a powerful technique for studying interactions between molecules and plasmonic nanostructures, it is interesting to consider the future directions for this technique in plasmonics. The challenge that has arisen in many of the studies presented here is the inherent coupling between molecular emission and the plasmon modes of the underlying substrate, which suggests that the location of the emission centroid does not necessarily correlate with the exact position of the molecule. However, we have shown that the emission centroid is related to the location of the molecule on the nanoparticle surface, given that the emission will only couple to local plasmon modes, which, in turn, dictates the position of the emission centroid.[20,21,62] In previous work, we showed that the SERS intensity, but not the centroid location, depends on the orientation of the molecule;[20] this result is consistent with work from Taminiau *et al.*[63] Understanding the exact relationship between the molecular position and orientation on the nanoparticle surface and how this affects the calculated centroid remains a major experimental and theoretical challenge for this field.

Despite this challenge, super-resolution imaging offers a unique tool for probing interactions between molecules and plasmonic nanostructures. By tuning both molecular and plasmon resonances, we can tune the strength of the plasmonic coupling and use super-resolution imaging to map how the emission centroid changes.[64,65] In the case of SEF, we also envision tuning the linker length between the fluorophore and the plasmonic substrate, in order to determine how the emission couples to the plasmon modes as the distance between the two species is increased.[66] We also believe that super-resolution imaging will be extremely powerful for studying site-specific binding of ligands to nanoparticle surfaces. A number of studies have suggested that ligands will preferentially bind to the ends of nanostructures, but the evidence for the site-specific binding has been indirect, based on linking nanostructures end-to-end and then imaging these resulting structures *via* SEM.[67,68] Using fluorescent tags and super-resolution imaging to localize ligand binding sites offers a direct route for studying the location of these sites, but there is an important catch: these studies must be performed in the limit where plasmon-coupling is minimized. Otherwise, the emission may occur far from the actual site of the bound molecule, as described above.[18]

Another challenge with super-resolution studies on plasmonic systems is the loss of associated spectral information. In our work, we have split the signal into two channels, one for super-resolution imaging and one for spectral acquisition.[20–22] However, Shi *et al.* have recently demonstrated a wavelength-resolved super-resolution imaging strategy, based on introducing a transmission grating at the output of their microscope.[69] The zero order grating mode collapses all photons into a single PSF, similar to the data presented in this perspective. However, the

first order grating mode disperses the light into its wavelength-resolved components, allowing the spectral identity of the emitter(s) to be determined. While the approach was demonstrated for fluorescent quantum dots, this type of instrumentation would be highly useful for studying plasmon-coupled emission processes. For example, Etchegoin and coworkers showed that different SERS bands appeared at slightly different spatial locations on a CCD detector but their resolution was limited by the diffraction-limit;[70,71] coupling wavelength-resolution with super-resolution optical imaging would be a powerful advance for studying interactions between molecules and plasmonic nanostructures.

To date, researchers have used a variety of clever techniques to introduce the signal modulation component of super-resolution imaging into plasmon-coupled emission processes; in this review, we described photoswitchable fluorophores,[18,24] catalytic turnovers,[7,26,27] and diffusion-limited processes.[19,25,72] In SERS, however, signal modulation presents a significant challenge, simply because the photophysics of a molecule adsorbed to a metal surface are vastly different than its photophysics in bulk solution. For this reason, a photoswitchable dye may not undergo the necessary structural rearrangements to behave as an effective photoswitch. However, catalysis may offer one unique strategy for overcoming this limitation. For example, Xie *et al.* have recently reported an Au–Pt–Au core–shell nanostructure that is both catalytically and SERS-active.[73] By using hybrid materials that have both SERS and catalytic activity, we may be able to follow reactions in a similar way to the experiments described by Chen and coworkers.[7,26,27] Electrochemical modulation presents another appealing strategy for modulating the SERS emission of an adsorbed dye, as described by Cortes *et al.*[74]

In summary, super-resolution imaging has opened new avenues of research in coupled molecule–plasmon systems that extend from ligand binding to catalysis to hot spot mapping. Given the superior spatial resolution (<5 nm) and the ability to directly image coupled emission processes, we expect super-resolution imaging to emerge as a highly complementary imaging strategy for studying plasmonic systems, with new analysis algorithms and wavelength-resolved images providing additional insight into this complex, yet important, system.

Acknowledgements

KAW gratefully acknowledges Eric Titus for help in preparing this manuscript. This material is based on work supported by the Welch Foundation under Award No. F-1699 and the Air Force Office of Scientific Research under AFOSR Award No. FA9550-09-0112.

References

1 R. Bardhan, S. Lal, A. Joshi and N. J. Halas, *Acc. Chem. Res.*, 2011, **44**, 936–946.
2 E. Boisselier and D. Astruc, *Chem. Soc. Rev.*, 2009, **38**, 1759–1782.
3 J. Kneipp, H. Kneipp and K. Kneipp, *Chem. Soc. Rev.*, 2008, **37**, 1052–1060.
4 T. Vo-Dinh, F. Yan and M. B. Wabuyele, *Top. Appl. Phys.*, 2006, **103**, 409–426.
5 J. N. Anker, W. P. Hall, O. Lyandres, N. C. Shah, J. Zhao and D. R. P. Van, *Nat. Mater.*, 2008, **7**, 442–453.
6 P. Christopher, H. Xin and S. Linic, *Nat. Chem.*, 2011, **3**, 467–472.
7 X. Zhou, N. M. Andoy, G. Liu, E. Choudhary, K.-S. Han, H. Shen and P. Chen, *Nat. Nanotechnol.*, 2012, **7**, 237–241.
8 E. C. Dreaden, A. M. Alkilany, X. Huang, C. J. Murphy and M. A. El-Sayed, *Chem. Soc. Rev.*, 2012, **41**, 2740–2779.
9 R. S. Golightly, W. E. Doering and M. J. Natan, *ACS Nano*, 2009, **3**, 2859–2869.
10 F. Casadio, M. Leona, J. R. Lombardi and D. R. Van, *Acc. Chem. Res.*, 2010, **43**, 782–791.
11 P. L. Stiles, J. A. Dieringer, N. C. Shah and R. P. Van Duyne, *Annu. Rev. Anal. Chem.*, 2008, **1**, 601–626.
12 C. D. Geddes, K. Aslan, I. Gryczynski, J. Malicka and J. R. Lakowicz, *Rev. Fluoresc.*, 2004, **1**, 365–401.
13 M. Moskovits, *J. Chem. Phys.*, 1978, **69**, 4159–4161.
14 E. C. Le Ru, M. Meyer, E. Blackie and P. G. Etchegoin, *J. Raman Spectrosc.*, 2008, **39**, 1127–1134.
15 A. M. Michaels, J. Jiang and L. Brus, *J. Phys. Chem. B*, 2000, **104**, 11965–11971.
16 K. A. Willets and R. P. Van Duyne, *Annu. Rev. Phys. Chem.*, 2007, **58**, 267–297.
17 E. C. Le Ru, J. Grand, N. Felidj, J. Aubard, G. Lelvi, A. Hohenau, J. R. Krenn, E. Blackie and P. G. Etchegoin, *J. Phys. Chem. C*, 2008, **112**, 8117–8121.
18 K. L. Blythe, K. M. Mayer, M. L. Weber and K. A. Willets, *Phys. Chem. Chem. Phys.*, 2012, DOI: 10.1039/C1032CP43152A.
19 S. M. Stranahan and K. A. Willets, *Nano Lett.*, 2010, **10**, 3777–3784.
20 E. J. Titus, M. L. Weber, S. M. Stranahan and K. A. Willets, *Nano Lett.*, 2012, **12**, 5103–5110.
21 M. L. Weber, J. P. Litz, D. J. Masiello and K. A. Willets, *ACS Nano*, 2012, **6**, 1839–1848.
22 M. L. Weber and K. A. Willets, *J. Phys. Chem. Lett.*, 2011, **2**, 1766–1770.
23 K. A. Willets, S. M. Stranahan and M. L. Weber, *J. Phys. Chem. Lett.*, 2012, **3**, 1286–1294.
24 H. Lin, S. P. Centeno, L. Su, B. Kenens, S. Rocha, M. Sliwa, J. Hofkens and H. Uji-i, *ChemPhysChem*, 2012, **13**, 973–981.
25 H. Cang, A. Labno, C. Lu, X. Yin, M. Liu, C. Gladden, Y. Liu and X. Zhang, *Nature*, 2011, **469**, 385–388.
26 W. Xu, J. S. Kong and P. Chen, *Phys. Chem. Chem. Phys.*, 2009, **11**, 2767–2778.
27 X. Zhou, W. Xu, G. Liu, D. Panda and P. Chen, *J. Am. Chem. Soc.*, 2010, **132**, 138–146.
28 M. L. Weber and K. A. Willets, *MRS Bull.*, 2012, **37**, 745–751.
29 M. J. Rust, M. Bates and X. Zhuang, *Nat. Methods*, 2006, **3**, 793–796.
30 E. Betzig, G. H. Patterson, R. Sougrat, O. W. Lindwasser, S. Olenych, J. S. Bonifacino, M. W. Davidson, J. Lippincott-Schwartz and H. F. Hess, *Science*, 2006, **313**, 1642–1645.

31 T. Huang and X.-H. N. Xu, *Nanoscale*, 2011, **3**, 3567–3572.
32 L. B. Sagle, L. K. Ruvuna, J. M. Bingham, C. Liu, P. S. Cremer and D. R. P. Van, *J. Am. Chem. Soc.*, 2012, **134**, 15832–15839.
33 F. Balzarotti and F. D. Stefani, *ACS Nano*, 2012, **6**, 4580–4584.
34 Y. Sivan, *Appl. Phys. Lett.*, 2012, **101**, 021111.
35 Y. Sivan, Y. Sonnefraud, S. Kena-Cohen, J. B. Pendry and S. A. Maier, *ACS Nano*, 2012, **6**, 5291–5296.
36 F. Wei and Z. Liu, *Nano Lett.*, 2010, **10**, 2531–2536.
37 W. E. Moerner, *J. Microsc.*, 2012, **246**, 213–220.
38 A. Yildiz, J. N. Forkey, S. A. McKinney, T. Ha, Y. E. Goldman and P. R. Selvin, *Science*, 2003, **300**, 2061–2065.
39 R. E. Thompson, D. R. Larson and W. W. Webb, *Biophys. J.*, 2002, **82**, 2775–2783.
40 M. P. Gordon, T. Ha and P. R. Selvin, *Proc. Natl. Acad. Sci. U. S. A.*, 2004, **101**, 6462–6465.
41 J. Foelling, M. Bossi, H. Bock, R. Medda, C. A. Wurm, B. Hein, S. Jakobs, C. Eggeling and S. W. Hell, *Nat. Methods*, 2008, **5**, 943–945.
42 C. Steinhauer, C. Forthmann, J. Vogelsang and P. Tinnefeld, *J. Am. Chem. Soc.*, 2008, **130**, 16840–16841.
43 K. Lidke, B. Rieger, T. Jovin and R. Heintzmann, *Opt. Express*, 2005, **13**, 7052–7062.
44 W. E. Moerner and D. P. Fromm, *Rev. Sci. Instrum.*, 2003, **74**, 3597–3619.
45 K. I. Mortensen, L. S. Churchman, J. A. Spudich and H. Flyvbjerg, *Nat. Methods*, 2010, **7**, 377–381.
46 J. Engelhardt, J. Keller, P. Hoyer, M. Reuss, T. Staudt and S. W. Hell, *Nano Lett.*, 2011, **11**, 209–213.
47 C. L. Haynes and D. R. P. Van, *J. Phys. Chem. B*, 2001, **105**, 5599–5611.
48 M. Frimmer, Y. Chen and A. F. Koenderink, *Phys. Rev. Lett.*, 2011, **107**, 123602.
49 T. Shegai, Y. Huang, H. Xu and M. Kaell, *Appl. Phys. Lett.*, 2010, **96**, 103114.
50 N. R. Jana, L. Gearheart and C. J. Murphy, *J. Phys. Chem. B*, 2001, **105**, 4065–4067.
51 Y. Fang, W.-S. Chang, B. Willingham, P. Swanglap, S. Dominguez-Medina and S. Link, *ACS Nano*, 2012, **6**, 7177–7184.
52 K. Watanabe, D. Menzel, N. Nilius and H.-J. Freund, *Chem. Rev.*, 2006, **106**, 4301–4320.
53 S. Linic, P. Christopher and D. B. Ingram, *Nat. Mater.*, 2011, **10**, 911–921.
54 H. Okamoto and K. Imura, *Prog. Surf. Sci.*, 2009, **84**, 199–229.
55 G. P. Wiederrecht, *Eur. Phys. J.: Appl. Phys.*, 2004, **28**, 3–18.
56 M. Rang, A. C. Jones, F. Zhou, Z.-Y. Li, B. J. Wiley, Y. Xia and M. B. Raschke, *Nano Lett.*, 2008, **8**, 3357–3363.
57 P. G. Etchegoin and E. C. Le Ru, *Phys. Chem. Chem. Phys.*, 2008, **10**, 6079–6089.
58 S. Nie and S. R. Emory, *Science*, 1997, **275**, 1102–1106.
59 J. A. Dieringer, R. B. Lettan II, K. A. Scheidt and R. P. Van Duyne, *J. Am. Chem. Soc.*, 2007, **129**, 16249–16256.
60 J. M. McMahon, S. Li, L. K. Ausman and G. C. Schatz, *J. Phys. Chem. C*, 2012, **116**, 1627–1637.
61 N. J. Halas, S. Lal, W.-S. Chang, S. Link and P. Nordlander, *Chem. Rev.*, 2011, **111**, 3913–3961.
62 L. K. Ausman and G. C. Schatz, *J. Chem. Phys.*, 2009, **131**, 084708.
63 T. H. Taminiau, F. D. Stefani, F. B. Segerink and H. N. F. Van, *Nat. Photonics*, 2008, **2**, 234–237.
64 A. D. McFarland, M. A. Young, J. A. Dieringer and R. P. Van Duyne, *J. Phys. Chem. B*, 2005, **109**, 11279–11285.
65 Y. Chen, K. Munechika and D. S. Ginger, *Nano Lett.*, 2007, **7**, 690–696.
66 J. R. Lakowicz, C. D. Geddes, I. Gryczynski, J. Malicka, Z. Gryczynski, K. Aslan, J. Lukomska, E. Matveeva, J. Zhang, R. Badugu and J. Huang, *J. Fluoresc.*, 2004, **14**, 425–441.
67 A. Lee, G. F. S. Andrade, A. Ahmed, M. L. Souza, N. Coombs, E. Tumarkin, K. Liu, R. Gordon, A. G. Brolo and E. Kumacheva, *J. Am. Chem. Soc.*, 2011, **133**, 7563–7570.
68 K. K. Caswell, J. N. Wilson, U. H. F. Bunz and C. J. Murphy, *J. Am. Chem. Soc.*, 2003, **125**, 13914–13915.
69 X. Shi, Z. Xie, Y. Song, Y. Tan, E. S. Yeung and H. Gai, *Anal. Chem.*, 2012, **84**, 1504–1509.
70 E. C. Le Ru and P. G. Etchegoin, *Chem. Phys. Lett.*, 2004, **396**, 393–397.
71 P. G. Etchegoin, E. C. Le Ru and A. Fainstein, *Phys. Chem. Chem. Phys.*, 2011, **13**, 4500–4506.
72 K. A. Willets and S. M. Stranahan, *Proc. SPIE*, 2012, **8228**, 82280P.
73 W. Xie, C. Herrmann, K. Koempe, M. Haase and S. Schluecker, *J. Am. Chem. Soc.*, 2011, **133**, 19302–19305.
74 E. Cortes, P. G. Etchegoin, E. C. Le Ru, A. Fainstein, M. E. Vela and R. C. Salvarezza, *Anal. Chem.*, 2010, **82**, 6919–6925.

